J Physiol Sci (2016) 66:127–142
DOI 10.1007/s12576-015-0404-5

ORIGINAL PAPER

Mechanisms of astrocytic K^+ clearance and swelling under high extracellular K^+ concentrations

Shingo Murakami[1,2] · **Yoshihisa Kurachi**[1,2]

Received: 15 June 2015 / Accepted: 16 September 2015 / Published online: 27 October 2015

Abstract In response to the elevation of extracellular K^+ concentration ($[K^+]_{out}$), astrocytes clear excessive K^+ to maintain conditions necessary for neural activity. K^+ clearance in astrocytes occurs via two processes: K^+ uptake and K^+ spatial buffering. High $[K^+]_{out}$ also induces swelling in astrocytes, leading to edema and cell death in the brain. Despite the importance of astrocytic K^+ clearance and swelling, the underlying mechanisms remain unclear. Here, we report results from a simulation analysis of astrocytic K^+ clearance and swelling. Astrocyte models were constructed by incorporating various mechanisms such as intra/extracellular ion concentrations of Na^+, K^+, and Cl^-, cell volume, and models of Na,K-ATPase, Na-K-Cl cotransporter (NKCC), K-Cl cotransporter, inwardly-rectifying K^+ (KIR) channel, passive Cl^- current, and aquaporin channel. The simulated response of astrocyte models under the uniform distribution of high $[K^+]_{out}$ revealed significant contributions of NKCC and Na,K-ATPase to increases of intracellular K^+ and Cl^- concentrations, and swelling. Moreover, we found that, under the non-uniform distribution of high $[K^+]_{out}$, KIR channels localized at synaptic clefts absorbed excess K^+ by depolarizing the equivalent potential of K^+ (E_K) above membrane potential, while K^+ released through perivascular KIR channels was enhanced by hyperpolarizing E_K and depolarizing membrane potential. Further analysis of simulated drug effects revealed that astrocyte swelling was modulated by blocking each of the ion channels and transporters. Our simulation analysis revealed controversial mechanisms of astrocytic K^+ clearance and swelling resulting from complex interactions among ion channels and transporters.

Keywords Kir 4.1 · Astrocyte · K^+ spatial buffering · Swelling

✉ Shingo Murakami
murakami@pharma2.med.osaka-u.ac.jp

Yoshihisa Kurachi
ykurachi@pharma2.med.osaka-u.ac.jp

[1] Division of Molecular and Cellular Pharmacology, Department of Pharmacology, Graduate School of Medicine, Osaka University, 2-2 Yamada-oka, Suita, Osaka 565-0871, Japan

[2] The Global Center for Medical Engineering and Informatics, Osaka University, 2-2 Yamada-oka, Suita, Osaka 565-0871, Japan

Introduction

Extracellular K^+ concentration ($[K^+]_{out}$) in the brain increases in response to ischemia, hypoxia, hypoglycemia, seizures, and spreading depression and can cause significant problems in brain function. Sustained exposure of neurons to elevated $[K^+]_{out}$ causes hyperexcitability and significant neuronal death [1–4]. In order to prevent the harmful elevation of $[K^+]_{out}$, astrocytes clear excessive K^+ in extracellular space (K^+ clearance) by redistributing K^+ from sites of high $[K^+]_{out}$ to those of low $[K^+]_{out}$ (K^+ spatial buffering). Two mechanisms of K^+ clearance are employed by astrocytes, referred to as K^+ uptake and K^+ release (Fig. 1a), in which astrocytes absorb excess extracellular K^+ (K^+ uptake) and release it to sites of low $[K^+]_{out}$ (K^+ release). However, K^+ uptake can result in astrocytic swelling, leading to the release of cytotoxic compounds which cause tissue damage and further cell swelling. The precise mechanisms that mediate K^+ clearance and swelling in astrocytes are not yet fully understood.

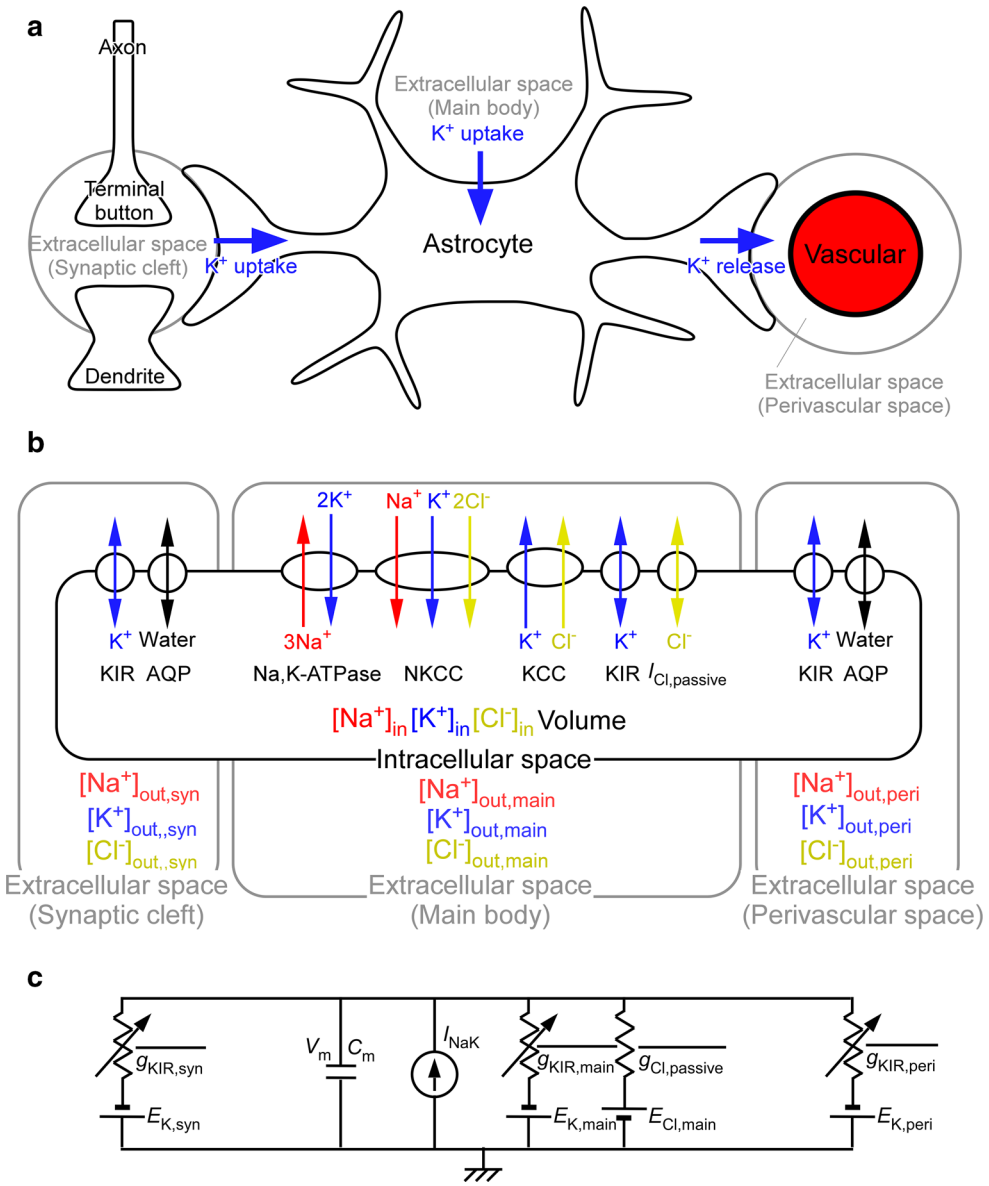

Fig. 1 Summary of the constructed astrocyte model. **a** The K^+ clearance mechanism in astrocytes, consisting of K^+ uptake and K^+ release. Excess K^+ in extracellular spaces surrounding the majority of the astrocytic membrane or synaptic cleft can be transferred into intracellular spaces (K^+ uptake). The absorbed K^+ in the intracellular space can be released into the extracellular part of the perivascular space (K^+ release), **b** schematic overview of the astrocyte model. The intracellular space of the astrocyte model was designed as one compartment with cell volume, $[Na^+]_{in}$, $[K^+]_{in}$, and $[Cl^-]_{in}$. The extracellular space surrounding the model was divided into three parts: synaptic cleft (*left*), main body (*center*), and perivascular space (*right*). Each of the extracellular spaces have their own $[Na^+]_{out}$, $[K^+]_{out}$, and $[Cl^-]_{out}$ independent from those in other extracellular spaces. Models of Na,K-ATPases, Na-K-Cl cotransporters (NKCCs), K-Cl cotransporters (KCCs), inwardly rectifying K^+ (KIR) channels, passive Cl^- current ($I_{Cl,passive}$), and aquaporin water (AQP) channels were incorporated into the compartment model, and **c** equivalent circuit of the constructed astrocyte model. Models of ion channels and electrogenic transporters (i.e. KIR channels, $I_{Cl,passive}$, and Na,K-ATPases) were incorporated into the equivalent circuit of the astrocytic membrane

Ion channels and transporters in astrocytes are thought to play important roles in K^+ clearance and swelling. Na,K-ATPase and Na-K-Cl cotransporter (NKCC) in astrocytes have been shown to contribute to K^+ clearance and high $[K^+]_{out}$-induced swelling [5–9]. In earlier studies, high K^+ conductance in astrocytes was found to produce K^+ spatial buffering [10, 11]. Recently, we reported that inwardly rectifying K^+ (KIR) channels containing KIR4.1 are differentially distributed in specific processes of astrocytes, such as the endfeet, and are colocalized with aquaporin (AQP) 4 channels in macrodomains [12–18]. Other groups have also shown that cells lacking KIR or

AQP channels exhibit reduced K^+ clearance and/or swelling [19–26]. However, their actual roles in these processes and the precise mechanisms by which they operate under high $[K^+]_{out}$ remain unknown.

Here, we investigate the mechanisms of astrocytic K^+ clearance and swelling by constructing astrocyte models with ion channels and transporters that are known to be involved in these processes, and reveal that these proteins have distinct roles in K^+ uptake and cell swelling. In addition, we provide evidence that perivascular KIR channels and those localized to the synaptic cleft have opposite roles in K^+ spatial buffering. We also theoretically show simulated block effects of ion channels and transporters on astrocytic swelling.

Methods

We developed astrocyte models that simulate the kinetics of membrane potential, ion and water flux through membranes, intra/extracellular ion concentrations, and cell volume (Fig. 1). To represent the localizations of KIR and AQP channels, we designed the membrane of the model to contain a main part, a synaptic part, and a perivascular part (Fig. 1b). Ion channels and transporters known to be related to ion and water transport in astrocytes were modeled and incorporated into the compartment model. By changing the flow of ions and water through the models of ion channels and transporters, high $[K^+]_{out}$, which occurs during high neuronal activity and disease, in the astrocyte models can cause changes in intracellular ion concentrations, electrochemical Na^+, K^+, and Cl^- gradients, membrane potential, and cell volume. Because regulatory volume decrease is usually observed with hypo-osmotic challenge and has not been consistently observed under high $[K^+]_{out}$ [9, 27], estemated regulatory volume decrease mechanisms after cell swelling (e.g., volume-sensitive outwardly rectifying Cl^- channel and volume-sensitive K^+ channel) were not considered in the present study. The equivalent circuit with ion channels and electrogenic transporters was also constructed to simulate membrane potential (Fig. 1c).

Basic structure of the constructed astrocyte models

The compartment model of an astrocyte was constructed with one intracellular space and three extracellular spaces, each of which was surrounded by one of three membranes (Fig. 1). The glossary and parameters in the model are summarized in Tables 1, 2, and 3. To represent localizations of KIR and AQP channels at endfeet surrounding the synapse and vascular space [15, 17, 18, 28, 29], the membrane of an astrocyte is divided into three parts: (1) the cell body and the majority of astrocytic processes (the main part), (2) perisynaptic processes that envelop the synapse (the synaptic part), and (3) the perivascular sheathing (vascular feet) that surrounds capillary walls (the perivascular part). All parts of the membrane in the model share the same membrane potential (V_m) and intracellular ion concentrations ($[Na^+]_{in}$, $[K^+]_{in}$ and $[Cl^-]_{in}$), whereas extracellular ion concentrations ($[Na^+]_{out}$, $[K^+]_{out}$ and $[Cl^-]_{out}$) are defined for each membrane independently. In the high $[K^+]_{out}$ simulation, only $[K^+]_{out}$ was elevated, while $[Cl^-]_{out}$ remained fixed and $[Na^+]_{out}$ was decreased to keep extracellular osmotic pressure constant. The total surface area of the synaptic part was set to 15 % of the whole membrane [30]. The total area of the perivascular part was calculated by assuming that an astrocyte has 10 peri-endfeet, with radii of 10 μm [31]. The total membrane capacitance included in the astrocyte model (C_m) was calculated by using the standard value of the unit capacity per area (1 μF/cm^2). Initial and resting intracellular ion concentrations were determined from experimental data [32–34] (Table 3). The kinetics of membrane potential and ion concentrations is described in the following equations:

$$\frac{dV_m}{dt} = \frac{\sum -I_{Na} - I_K - I_{Cl}}{C_m} \quad (1)$$

$$\frac{d[Na^+]_{in}}{dt} = \frac{\sum -I_{Na}}{F \cdot Vol} \quad (2)$$

$$\frac{d[K^+]_{in}}{dt} = \frac{\sum -I_K}{F \cdot Vol} \quad (3)$$

$$\frac{d[Cl^-]_{in}}{dt} = \frac{\sum I_{Cl}}{F \cdot Vol} \quad (4)$$

$$\frac{dVol}{dt} = J_{water} \quad (5)$$

where V_m is the membrane potential, I_i is the ionic current of ion i in each compartment, F is the Faraday constant, Vol is the total volume of the astrocyte, and J_{water} is the water flux. The outward ionic current and inward water flux are defined as positive. The ionic currents are calculated by summing ionic currents through the ion channels and transporters as follows:

$$I_{Na} = I_{Na,NaK} + I_{Na,NKCC} \quad (6)$$

$$I_{KIR} = I_{KIR,syn} + I_{KIR,main} + I_{KIR,peri} \quad (7)$$

$$I_K = I_{K,NaK} + I_{K,NKCC} + I_{KIR} \quad (8)$$

$$I_{Cl} = I_{Cl,NKCC} + I_{Cl,passive} \quad (9)$$

where $I_{i,j}$ is the current of ion i through ion channels or transporters (j) and $I_{K,KIR,k}$ is the current through the KIR channel at k ('syn', 'main', and 'peri' for the synaptic cleft, main part, and the perivascular part, respectively).

Table 1 Glossary

Symbol	Definition	Unit
$[Na^+]_{in}$	Intracellular Na^+ concentration	mM
$[K^+]_{in}$	Intracellular K^+ concentration	mM
$[Cl^-]_{in}$	Intracellular Cl^- concentration	mM
$[Na^+]_{out,syn}$	Extracellular Na^+ concentration in the synaptic cleft	mM
$[K^+]_{out,syn}$	Extracellular K^+ concentration in the synaptic cleft	mM
$[Cl^-]_{out,syn}$	Extracellular Cl^- concentration in the synaptic cleft	mM
$[Na^+]_{out,main}$	Extracellular Na^+ concentration outside of the main part	mM
$[K^+]_{out,main}$	Extracellular K^+ concentration outside of the main part	mM
$[Cl^-]_{out,main}$	Extracellular Cl^- concentration outside of the main part	mM
$[Na^+]_{out,peri}$	Extracellular Na^+ concentration in the perivascular space	mM
$[K^+]_{out,peri}$	Extracellular K^+ concentration in the perivascular space	mM
$[Cl^-]_{out,peri}$	Extracellular Cl^- concentration in the perivascular space	mM
$[Total]_{in}$	Total concentration of $[Na^+]_{in}$ $[K^+]_{in}$ and $[Cl^-]_{in}$	mM
$[Total]_{out,syn}$	Total concentration of $[Na^+]_{out,syn}$ $[K^+]_{out,syn}$ and $[Cl^-]_{out,syn}$	mM
$[Total]_{out,main}$	Total concentration of $[Na^+]_{out,main}$ $[K^+]_{out,main}$ and $[Cl^-]_{out,main}$	mM
$[Total]_{out,peri}$	Total concentration of $[Na^+]_{out,peri}$ $[K^+]_{out,peri}$ and $[Cl^-]_{out,peri}$	mM
I_{Na}	Na^+ current	pA
I_K	K^+ current	pA
I_{Cl}	Cl^- current	pA
V_m	Membrane potential	mV
C_m	Membrane capacitance	pF
A_{syn}	Area of the astrocytic membrane around the synaptic cleft	μm^2
A_{main}	Area of the astrocytic membrane of the main part	μm^2
A_{peri}	Area of the astrocytic membrane around the perivascular space	μm^2
Vol	Total volume in the astrocyte model	μm^3
Vol_{org}	Initial Vol	μm^3
R	Gas constant	J/(K mol)
T	Temperature	K
F	Faraday constant	C/mol
I_{NaK}	Total current flowing through the Na,K-ATPase	pA
$\overline{I_{NaK}}$	Maximum current factor flowing through the Na,K-ATPase	$pA/\mu m^2$
$I_{Na,NaK}$ I_{Na}	flowing through the Na,K-ATPase	pA
$I_{K,NaK}$ I_K	flowing through the Na,K-ATPase	pA
f_{NaK}	Voltage-dependent parameter for the I_{NaKATP}	1
σ	$[Na^+]_o$-dependent factor for I_{NaKATP}	1
$I_{Na,NKCC}$	I_{Na} through the NKCC	pA
$I_{K,NKCC}$	I_K through the NKCC	pA
$I_{Cl,NKCC}$	I_{Cl} through the NKCC	pA
I_{NKCC}	Total current through the NKCC	pA
$\overline{I_{NKCC}}$	Factor defining the maximum ionic flux through the NKCC	pA ms/μm^2
y	Probability of the five E_1 states	1
α_{NKCC}	Rate constant for y	1/ms
β_{NKCC}	Rate constant for y	1/ms
kf_{Full}	Forward rate constant for the ion-filled cotransporter	1/ms
kb_{Full}	Backward rate constants for the ion-filled cotransporter	1/ms
kf_{Empty}	Forward rate constant for the empty form	1/ms
kb_{Empty}	Backward rate constant for the empty form	1/ms
$p(E_{1NaClKCl})$	Probabilities of $E_{1NaClKCl}$ within the total five states of E_1	1

Table 1 continued

Symbol	Definition	Unit
$p(E_1)$	Probabilities of E_1 within the total five states of E_1	1
$p(E_{2NaClKCl})$	Probabilities of $E_{2NaClKCl}$ within the total five states of E_2	1
$p(E_2)$	Probabilities of E_2 within the total five states of E_2	1
K_{Na}	Binding constant for Na^+ in the NKCC	1/mM
K_K	Binding constant for K^+ in the NKCC	1/mM
K_{Cl}	Binding constant for Cl^- in the NKCC	1/mM
I_{KCC}	Total current through the KCC	pA
$\overline{I_{KCC}}$	Factor defining ion flux through the KCC	pA/μm^2
$I_{K,KCC}$	I_K through the KCC	pA
$I_{Cl,KCC}$	I_{Cl} through the KCC	pA
I_{KIR}	I_K through the KIR channel	pA
$I_{KIR,syn}$	I_{KIR} through the astrocytic membrane around synaptic cleft	pA
$I_{KIR,main}$	I_{KIR} through the astrocytic membrane around the main part	pA
$I_{KIR,peri}$	I_{KIR} through the astrocytic membrane in the perivascular space	pA
$\overline{g_{KIR,syn}}$	Maximum conductance for $I_{KIR,syn}$	pA/M$^{1/2}$ μm^2 mV
$\overline{g_{KIR,main}}$	Maximum conductance for $I_{KIR,main}$	pA/M$^{1/2}$ μm^2 mV
$\overline{g_{KIR,peri}}$	Maximum conductance for $I_{KIR,peri}$	pA/M$^{1/2}$ μm^2 mV
$E_{K,syn}$	Equivalent potential for K^+ in the astrocytic membrane around the synaptic cleft	mV
$E_{K,main}$	Equivalent potential for K^+ in the astrocytic membrane around the main part	mV
$E_{K,peri}$	Equivalent potential for K^+ in the astrocytic membrane in the perivascular space	mV
$I_{Cl,passive}$	Passive Cl^- current	pA
$\overline{g_{Cl,passive}}$	Maximum conductance for $I_{Cl,passive}$	pA/μm^2 mV
$E_{Cl,main}$	Equivalent potential for Cl^-in the astrocytic membrane around the main part	mV
J_{water}	Water flux	μm^3/s
$F_{tension}$	Equivalent concentration of force for restoring the cell to its original volume	mM
$\overline{g_{water,syn}}$	Maximum hydraulic conductance in the astrocytic membrane around the synaptic cleft	μm mol/s mM J
$\overline{g_{water,main}}$	Maximum hydraulic conductance in the astrocytic membrane around the main par	μm mol/s mM J
$\overline{g_{water,peri}}$	Maximum hydraulic conductance in the astrocytic membrane in the perivascular space	μm mol/s mM J
$\overline{K_{tension}}$	Factor defining the force for restoring the cell to its original volume	mM/μm^3

Models of ion channels and transporters

Na,K-ATPases

We adopted the Na,K-ATPase model developed by Luo and Rudy [35] to simulate the current through Na,K-ATPases. The current through Na,K-ATPases was expressed using the following equations:

$$I_{NaK} = \overline{I_{NaK}} \cdot A_{main} \cdot \frac{f_{NaK}}{1 + \left(\frac{10}{[Na^+]_{in}}\right)^2} \cdot \frac{1}{1 + \frac{1.5}{[K^+]_{out,main}}} \quad (10)$$

$$f_{NaK} = \frac{1}{1 + 0.1245 \cdot e^{\left(\frac{-0.1 \cdot V_m \cdot F}{RT}\right)} + 0.0365 \cdot \delta \cdot e^{\left(\frac{-V_m \cdot F}{RT}\right)}} \quad (11)$$

$$\delta = \frac{e^{\left(\frac{[Na^+]_{out,main}}{67.3}\right)} - 1}{7} \quad (12)$$

where I_{NaK} is the total current through the Na,K-ATPase, $\overline{I_{NaK}}$ is the maximum current factor, A_{main} is the membrane area of the main part, f_{NaK} is the voltage-dependent parameter for the I_{NaK}, and σ is the $[Na^+]_{out}$-dependent factor for I_{NaK}. An Na,K-ATPase pumps three Na^+ ions out of a cell for every two K^+ ions pumped in. Therefore, each ionic current can be described by the following equations:

$$I_{Na,NaK} = 3 \cdot I_{NaK} \quad (13)$$

$$I_{K,NaK} = -2 \cdot I_{NaK} \quad (14)$$

where $I_{i,NaK}$ is the current of ion i flowing through the Na,K-ATPase.

NKCCs

To simulate ionic flows through NKCCs in astrocytes, we adopted a NKCC model based on a two-state Markov-type

Table 2 Model constants

Symbol	Value	Unit
$[Na^+]_{out}$	135 (control)	mM
$[K^+]_{out}$	3 (control)	mM
$[Cl^-]_{out}$	138	mM
A_{syn}	6750.0	μm^2
A_{main}	37,464.6	μm^2
A_{peri}	785.4	μm^2
Vol_{org}	3000	μm^3
R	8.31	J/(K mol)
T	310	K
F	96,485	C/mol
$\overline{I_{NaK}}$	1.8×10^{-4}	$pA/\mu m^2$
$\overline{I_{NKCC}}$	1.5×10^{1}	pA ms/μm^2
kf_{Full}	3.1	1/ms
kb_{Full}	1.5	1/ms
kf_{Empty}	37.8	1/ms
kb_{Empty}	79.5	1/ms
K_{Na}	8.4×10^{-2}	1/mM
K_K	1.2×10^{-3}	1/mM
K_{Cl}	5.7×10^{-2}	1/mM
$\overline{I_{KCC}}$	4.4×10^{-5}	$pA/\mu m^2$
$\overline{g_{KIR,syn}}$	4.4×10^{-6}	$pA/M^{1/2}\ \mu m^2$ mV
$\overline{g_{KIR,main}}$	4.4×10^{-7}	$pA/M^{1/2}\ \mu m^2$ mV
$\overline{g_{KIR,peri}}$	4.4×10^{-5}	$pA/M^{1/2}\ \mu m^2$ mV
$\overline{g_{Cl,passive}}$	9.3×10^{-7}	$pA/\mu m^2$ mV
$\overline{g_{water,syn}}$	5.0×10^{-8}	μm mol/s mM J
$\overline{g_{water,main}}$	0	μm mol/s mM J
$\overline{g_{water,peri}}$	5.0×10^{-8}	μm mol/s mM J
$\overline{K_{tension}}$	0.12	$mM/\mu m^3$

Table 3 Initial and resting conditions

Symbol	Initial value	Unit
$[Na^+]_{in}$	15	mM
$[K^+]_{in}$	130	mM
$[Cl^-]_{in}$	100	mM
V_m	−90	mV
Vol	3000	μm^3

model simplified from Benjamin's model (Fig. 2a) [36, 37]. In this model, the transport direction and turnover rate in the NKCC model are determined by the intracellular and extracellular ion concentrations. The E_1 and E_2 states in the NKCC model represent the fractions having their ion-binding sites on the external and internal side, respectively. The probabilities of the E_1 state and E_2 state are represented by y and $(1 - y)$. The steady state of y was calculated as follows:

$$y = \frac{\beta_{NKCC}}{\alpha_{NKCC} + \beta_{NKCC}} \tag{15}$$

where α_{NKCC} and β_{NKCC} are the rate constants, respectively. These constants are given by following equations:

$$\alpha_{NKCC} = kf_{Full} \cdot p(E_{1NaClKCl}) + kb_{Empty} \cdot p(E_1) \tag{16}$$

$$\beta_{NKCC} = kb_{Full} \cdot p(E_{2NaClKCl}) + kf_{Empty} \cdot p(E_2) \tag{17}$$

where kf_{Full} and kb_{Full} are the forward and backward rate constants for the ion-filled cotransporter, kf_{Empty} and kb_{Empty} are the forward and backward rate constants for the empty form, $p(E_{1NaClKCl})$ and $p(E_1)$ are the probabilities of $E_{1NaClKCl}$ and E_1 within the total five states of E_1, and $p(E_{2NaClKCl})$ and $p(E_2)$ are the probabilities of $E_{2NaClKCl}$ and E_2 within the total five states of E_2. The $p(E_1)$, $p(E_{1NaClKCl})$, $p(E_2)$, and $p(E_{2NaClKCl})$ are given by:

$$p(E_1) = \frac{1}{\begin{pmatrix} 1 + K_{Na} \cdot [Na^+]_{out,main} + K_{Na} \cdot [Na^+]_{out,main} \cdot K_{Cl} \cdot [Cl^-]_{out,main} \\ + K_{Na} \cdot [Na^+]_{out,main} \cdot K_{Cl} \cdot [Cl^-]_{out,main} \cdot K_K \cdot [K^+]_{out,main} \\ + K_{Na} \cdot [Na^+]_{out,main} \cdot K_{Cl} \cdot [Cl^-]_{out,main} \cdot K_K \cdot [K^+]_{out,main} \cdot K_{Cl} \cdot [Cl^-]_{out,main} \end{pmatrix}} \tag{18}$$

$$p(E_{1NaClKCl}) = K_{Na} \cdot [Na^+]_{out,main} \cdot K_{Cl} \cdot [Cl^-]_{out,main} \cdot K_K \cdot [K^+]_{out,main} \cdot K_{Cl} \cdot [Cl^-]_{out,main} \cdot p(E_1) \tag{19}$$

$$p(E_2) = \frac{1}{\begin{pmatrix} 1 + K_{Cl} \cdot [Cl^-]_{in} + K_K \cdot [K^+]_{in} \cdot K_{Cl} \cdot [Cl^-]_{in} \\ + K_{Cl} \cdot [Cl^-]_{in} \cdot K_K \cdot [K^+]_{in} \cdot K_{Cl} \cdot [Cl^-]_{in} \\ + K_{Na} \cdot [Na^+]_{in} \cdot K_{Cl} \cdot [Cl^-]_{in} \cdot K_K \cdot [K^+]_{in} \cdot K_{Cl} \cdot [Cl^-]_{in} \end{pmatrix}} \tag{20}$$

$$p(E_{2NaClKCl}) = K_{Na} \cdot [Na^+]_{in} \cdot K_{Cl} \cdot [Cl^-]_{in} \cdot K_K \cdot [K^+]_{in} \cdot K_{Cl} \cdot [Cl^-]_{in} \cdot p(E_2) \tag{21}$$

where K_i is the binding constant for ion i.

Ion flux through the NKCC can be calculated by the following equations:

$$I_{NKCC} = 0 \tag{22}$$

$$I_{Na,NKCC} = -\overline{I_{NKCC}} \cdot A_{main} \cdot (p(E_{1NaClKCL}) \cdot y \cdot kf_{Full} - p(E_{2NaClKCL}) \cdot (1 - y) \cdot kb_{Full}) \tag{23}$$

$$I_{K,NKCC} = -\overline{I_{NKCC}} \cdot A_{main} \cdot (p(E_{1NaClKCL}) \cdot y \cdot kf_{Full} - p(E_{2NaClKCL}) \cdot (1 - y) \cdot kb_{Full}) \tag{24}$$

$$I_{Cl,NKCC} = 2 \cdot \overline{I_{NKCC}} \cdot A_{main} \cdot (p(E_{1NaClKCL}) \cdot y \cdot kf_{Full} - p(E_{2NaClKCL}) \cdot (1 - y) \cdot kb_{Full}) \tag{25}$$

where I_{NKCC} is the total current through the NKCC, $\overline{I_{NKCC}}$ is the factor defining the maximum ionic flux through the NKCC and $I_{i,NKCC}$ is the current of ion i through the NKCC.

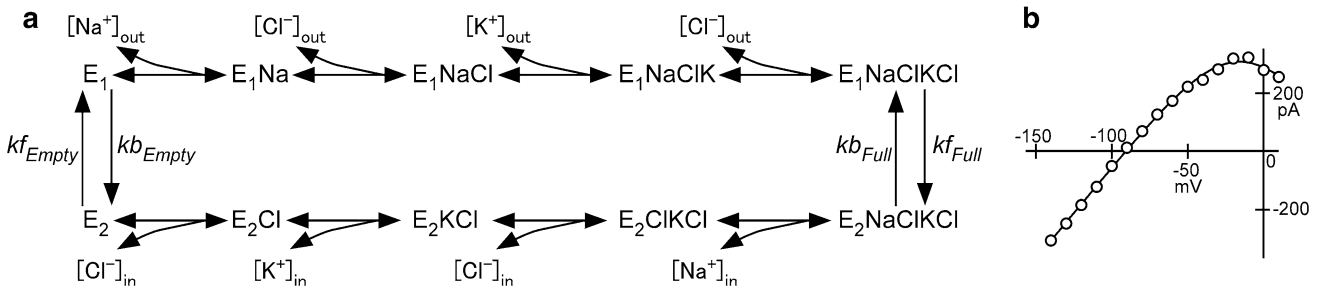

Fig. 2 A schema for the NKCC model and current–voltage relationship of the KIR model. **a** A schema for the NKCC model of Markov-type simplified from Benjamin's model [36, 37]. *E*1 and *E*2 in the model represent the states having their ion-binding sites on the extracellular and intracellular sides, respectively. Each of *E*1 and *E*2 state consists of five states according to the sequential binding of Na^+, Cl^-, K^+ and Cl^-. The translocation between *E*1 and *E*2 can happen only between the fully occupied states (E_1NaClkCl and E_2NaClKCl) or between empty states (E_1 and E_2), and **b** the current–voltage relationship of I_{KIR} in the KIR model. The current–voltage relationship with Eq. (29) (*solid line*) is shown with the experimental I_{KIR} in astrocytes (*circle*) [41]

KCCs

There have been no full kinetic models of KCC activity that provide a complete set of binding and translocation parameters [38]. Therefore, we adopted the KCC model in a Nernst-like fashion [39], which can reproduce bidirectional ion flux according to the balance between intracellular and extracellular ion concentrations [40]. The ionic currents through the KCC are described by:

$$I_{KCC} = 0 \tag{26}$$

$$I_{K,KCC} = -\overline{I_{KCC}} \cdot A_{main} \cdot \ln\left(\frac{[K^+]_{out,main} \cdot [Cl^-]_{out,main}}{[K^+]_{in} \cdot [Cl^-]_{in}}\right) \tag{27}$$

$$I_{Cl,KCC} = \overline{I_{KCC}} \cdot A_{main} \cdot \ln\left(\frac{[K^+]_{out,main} \cdot [Cl^-]_{out,main}}{[K^+]_{in} \cdot [Cl^-]_{in}}\right) \tag{28}$$

where I_{KCC} is the total current through the KCC, $\overline{I_{KCC}}$ is a factor defining ion flux through the KCC, and $I_{i,KCC}$ is the ionic current of ion i through the KCC.

KIR channels

The current–voltage (I–V) relationship of the KIR current in astrocytes was taken from experimental data [41] and was fitted to the Boltzmann function (Fig. 2b). The KIR current was calculated using the following equation:

$$I_{KIR,i} = \overline{g_{KIR,i}} \cdot A_i \cdot \sqrt{[K]_{out,i}} \cdot \left(\frac{1}{1 + e^{\frac{V_m - E_{K,i} - 91.7}{25.6}}}\right) \cdot \left(V_m - E_{K,i}\right) \tag{29}$$

where i is syn, main, or peri for synaptic part, main part, and perivascular part, respectively, $I_{KIR,i}$ is the KIR current of part i, $\overline{g_{KIR,i}}$ is the maximum conductance for I_{KIR} in part i, A_i is the membrane area of part i, and $E_{K,i}$ is the equivalent potential for K^+ in part i.

Passive Cl^- current

The I–V relationship of the passive Cl^- current in normal astrocytes [42, 43] is represented by the following equation:

$$I_{Cl,passive} = \overline{g_{Cl,passive}} \cdot A_{main} \cdot (V_m - E_{Cl,main}) \tag{30}$$

where $I_{Cl,passive}$ is the passive Cl^- current, $\overline{g_{Cl,passive}}$ is the maximum conductance for $I_{Cl,passive}$, and $E_{Cl,main}$ is the equivalent potential for Cl^- at the astrocytic membrane around the main part.

AQP channels

The flux of water through the membrane by the osmotic difference is given by the following equations [44]:

$$J_{water} = \sum_{\cdot T} \overline{g_{water,i}} \cdot A_i \cdot \left([Total]_{in} - [Total]_{out,i} - F_{tension}\right) \cdot R \tag{31}$$

$$[Total]_{in} = [Na^+]_{in} + [K^+]_{in} + [Cl^-]_{in} + 31.0 \tag{32}$$

$$[Total]_{out,i} = [Na^+]_{out,i} + [K^+]_{out,i} + [Cl^-]_{out,i} \tag{33}$$

$$F_{tension} = \overline{K_{tension}} \cdot \left(Vol - Vol_{org}\right) \tag{34}$$

where J_{water} is the water flux, $\overline{g_{water,i}}$ is the hydraulic conductivity for part i, and $[Total]_{in}$ is the sum of ion concentrations in intracellular space, $[Total]_{out,i}$ is the sum of ion concentrations in extracellular space of i, $[Na^+]_{out,i}$ is the extracellular Na^+ concentration outside of part *i*, $[K^+]_{out,i}$ is the extracellular K^+ concentration outside of part *i*, $[Cl^-]_{out,i}$ is the extracellular Cl^- concentration outside of part i, $F_{tension}$ is the equivalent concentration of elastic force of cytoskeleton that change the cell volume toward the original volume, *R* is the Gas constant, *T* is the absolute temperature, $\overline{K_{tension}}$ is the factor defining $F_{tension}$, Vol is

the volume of the astrocyte mode and Vol_{org} is the initial value of Vol.

Maximum conductance and current densities

The maximum conductance and current densities for the ion channels and transporters were determined using equilibrium state, in which no ionic currents flow at steady and initial states. Values for the other maximum conductance and current densities were determined by solving a system of equations:

$$I_{Na,NaK} + I_{Na,NKCC} = 0 \quad (35)$$

$$I_{K,NaK} + I_{K,NKCC} + I_{K,KCC} + I_{KIR} = 0 \quad (36)$$

$$I_{Cl,NKCC} + I_{Cl,KCC} + I_{Cl,passive} = 0 \quad (37)$$

and Eqs. (13), (14), (22)–(28). KIR channels in astrocytes are localized in the membrane surrounding the synaptic cleft and perivascular space [15, 17, 18, 28, 29]. Therefore, the maximum conductance of KIR channels in the synaptic cleft and perivascular space was increased, while the total KIR channel current was kept constant.

Results

Simulation of high $[K^+]_{out}$-induced increases in intracellular ion concentrations and swelling

In the presence of high $[K^+]_{out}$, astrocytes have been shown to absorb extracellular K^+ and undergo swelling [5–9, 45]. To study the underlying mechanisms of these processes, we constructed astrocyte models based on a variety of experimental data. We first used the constructed models to reproduce high $[K^+]_{out}$-induced increases in astrocytic intracellular ion concentrations and swelling (Fig. 3).

In the first simulation, we assumed that high $[K^+]_{out}$ was applied to all parts of an isolated astrocyte. When the applied $[K^+]_{out}$ was increased from 3 to 20 mM over a 10-min period (Fig. 3a, $[K^+]_{out,all}$), the simulated cell volume increased (Fig. 3a, Volume). Cell volume reached 3596.7 μm^3 after 10 min, representing a 19.9 % increase; following a washout of K^+, cell volume gradually returned to levels matching those in controls. This response is similar to those reported in previous experimental studies [9, 27]. Cell swelling in the astrocyte model was nearly proportional to the levels of $[K^+]_{out}$ (Fig. 3b, Volume). The simulated swelling was due to the constant influx of water through AQP channels during the period of high $[K^+]_{out}$ (Fig. 3a, Water flux), caused by increased intracellular concentrations. As estimated from previously published experiments [32, 46–48], the simulated intracellular concentrations of K^+ and Cl^- ($[K^+]_{in}$ and $[Cl^-]_{in}$) increased sharply upon elevation of $[K^+]_{out}$, settling at levels of 152.0 and 139.8 mM, respectively (Fig. 3a, $[K^+]_{in}$, $[Cl^-]_{in}$). In contrast, high $[K^+]_{out}$ led to a slight change of $[Na^+]_{in}$ during the $[K^+]_{out}$ period (Fig. 3a, $[Na^+]_{in}$) as seen in a study by Rose & Ransom [32]. The incremental changes in $[K^+]_{in}$ and $[Cl^-]_{in}$ increased the intracellular osmotic pressure and thereby the influx of water through the AQP channels. The increase in volume due to this influx of water can attenuate the increases in $[K^+]_{in}$, $[Cl^-]_{in}$, and intracellular osmotic pressure. Therefore, the influx of water continued until intracellular osmotic pressure equilibrated with the sum of the extracellular osmotic pressure and elastic force returning to the original cell volume. Increases of $[K^+]_{in}$ and $[Cl^-]_{in}$ were also nearly proportional to increases of $[K^+]_{out}$ (Fig. 3b, $[K^+]_{in}$, $[Cl^-]_{in}$). This explains why increases of water influx (Fig. 3b, Water flux) and cell volume (Fig. 3b, Volume) are proportional to increases in high $[K^+]_{out}$. Taken together, these results demonstrate that the constructed astrocyte models successfully reproduced the previously reported characteristic increases of $[K^+]_{in}$ and $[Cl^-]_{in}$ and astrocyte swelling observed under high $[K^+]_{out}$, even without needing to arbitrarily adjust the parameters used in the model to reproduce such effects.

Contribution of astrocytic ion channels and transporters to high $[K^+]_{out}$-induced increases of astrocytic intracellular ion concentrations and swelling

Based on experimental results, various mechanisms have been proposed to account for astrocytic K^+ uptake and swelling [49, 50]. To elucidate potential underlying mechanisms, we further analyzed processes associated with the simulated high $[K^+]_{out}$-induced effects on intracellular ion concentrations shown in Fig. 3a. In this analysis, ionic flux through membrane ion channels and transporters were examined separately (Fig. 4).

The ionic fluxes of Na^+, K^+, and Cl^- under 20 mM $[K^+]_{out}$ conditions are shown in Fig. 4 and Table 4. Following the application of 20 mM $[K^+]_{out}$, Na^+ initially flowed into the intracellular space, but Na^+ flow was attenuated and then ceased (Fig. 4). K^+ and Cl^- also initially flowed inward. However, after K^+ and Cl^- flow was attenuated, K^+ and Cl^- flow did not cease. This difference in ionic flows is responsible for the observed significant increases in $[K^+]_{in}$ and $[Cl^-]_{in}$ and slight increase of $[Na^+]_{in}$.

Next, we examined ionic flow through each of the classes of ion channels and transporters in the astrocytic membrane. Na^+ flux in the astrocyte model was accounted for by Na,K-ATPase and NKCC (Fig. 4, Na^+ flux). In the control, the total flux of Na^+ was balanced by the efflux through Na,K-ATPases and influx through NKCCs, similar

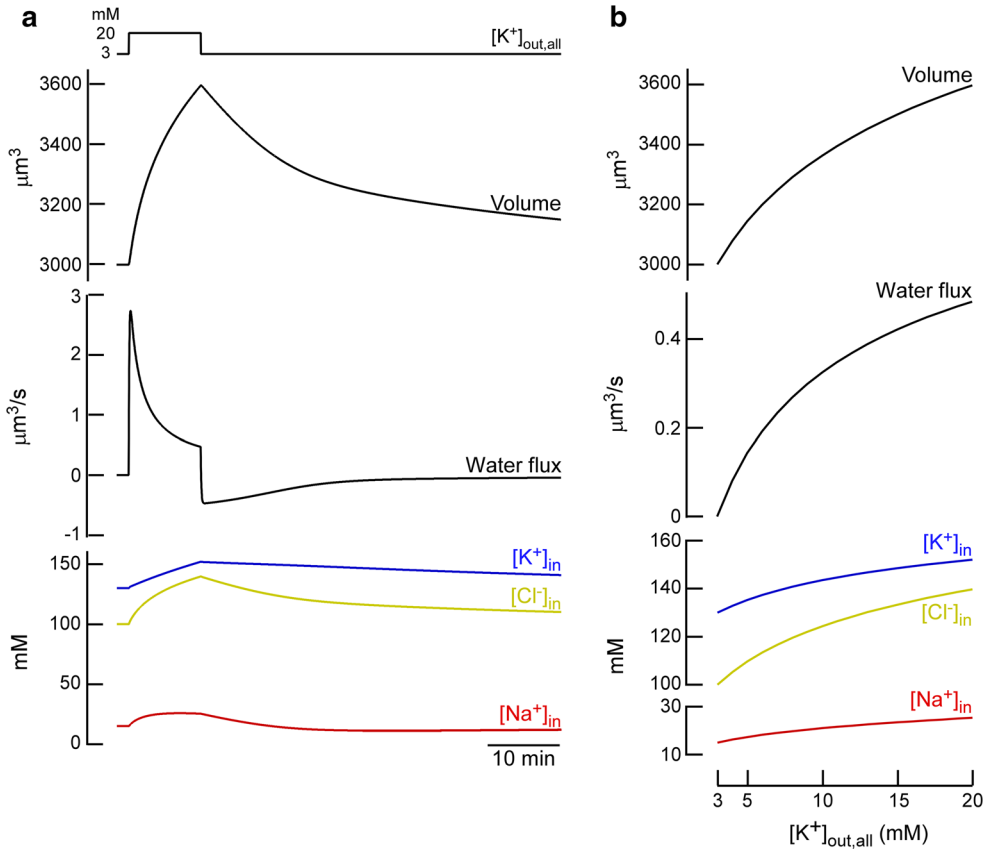

Fig. 3 Simulated effects of high $[K^+]_{out}$ on astrocytes. **a** The simulated effects of high $[K^+]_{out}$ on the astrocyte model: 20 mM K^+ was applied to all membranes of the astrocyte model for 10 min as shown in the protocol of applied $[K^+]_{out}$ (*row 1*). Simulated cell volume changes (*row 2*), water flux through membranes (*row 3*), and intracellular ion concentrations (i.e. $[Na^+]_{in}$, $[K^+]_{in}$, $[Cl^-]_{in}$) (*row 4*) are shown. Positive values in *row 3* correspond to an influx of water, and **b** the simulated effects of different $[K^+]_{out}$ levels on the astrocyte model: the effects of various $[K^+]_{out}$ levels (3–20 mM) were calculated at the end of 10-min sessions; the results are shown for cell volume (*row 1*), water flux (*row 2*), and intracellular ion concentration (*row 3*)

to Na^+ recycling previously observed in the epithelium (Table 5, Na^+ flux) [51–53]. Upon elevation of $[K^+]_{out}$, the activity of NKCCs was increased so that Na^+, together with K^+ and Cl^-, flowed into the intracellular space. However, the increase in Na^+ influx was countered by an increase of Na^+ efflux though Na,K-ATPases, the activity of which increased with increased levels $[K^+]_{out}$. This shows that relatively small changes in $[Na^+]_{in}$ could be accounted for by the balance between the enhanced efflux through Na,K-ATPases and influx through NKCCs (Table 4, Na^+ flux).

The K^+ flux in the astrocyte model was accounted for by investigating the activity of Na,K-ATPases, NKCCs, K-Cl cotransporters (KCCs), and KIR channels (Fig. 4, K^+ flux; Table 4). In the control model, the total flux of K^+ was balanced by the influx through Na,K-ATPases and NKCCs, and the efflux through KCCs and KIR channels (Table 5, K^+ flux). Following elevation of $[K^+]_{out}$, enhanced activity of Na,K-ATPases and NKCCs resulted in the absorption of excess extracellular K^+ into the intracellular space (Fig. 4, K^+ flux). The inward uptake of K^+ through NKCCs was initially strong, and slowed to a steady rate of K^+ influx. In contrast, the efflux of K^+ through KCCs and KIR channels was suppressed following the elevation of $[K^+]_{out}$. The contributions of KCCs and KIR channels to enhanced K^+ influx are smaller (Table 4, K^+ flux). Therefore, we conclude that K^+ absorption by astrocytes under high $[K^+]_{out}$ conditions can be primarily accounted for by increases in influx through Na,K-ATPases and NKCCs.

The Cl^- flux in the astrocyte model was determined by calculating the activities of NKCCs and KCCs and changes in the passive Cl^- current ($I_{Cl,passive}$; Fig. 4, Cl^- flux). In the control simulation, Cl^- flux was balanced by the influx through NKCCs and efflux through KCCs, and $I_{Cl,passive}$ (Table 5, Cl^- flux). The elevation of $[K^+]_{out}$ resulted in an increase of Cl^- influx through NKCCs, as noted above for Na^+ and K^+, and decreases in the efflux through KCCs and $I_{Cl,passive}$, although these changes were comparatively minimal (Table 4, Cl^- flux). This revealed that elevated

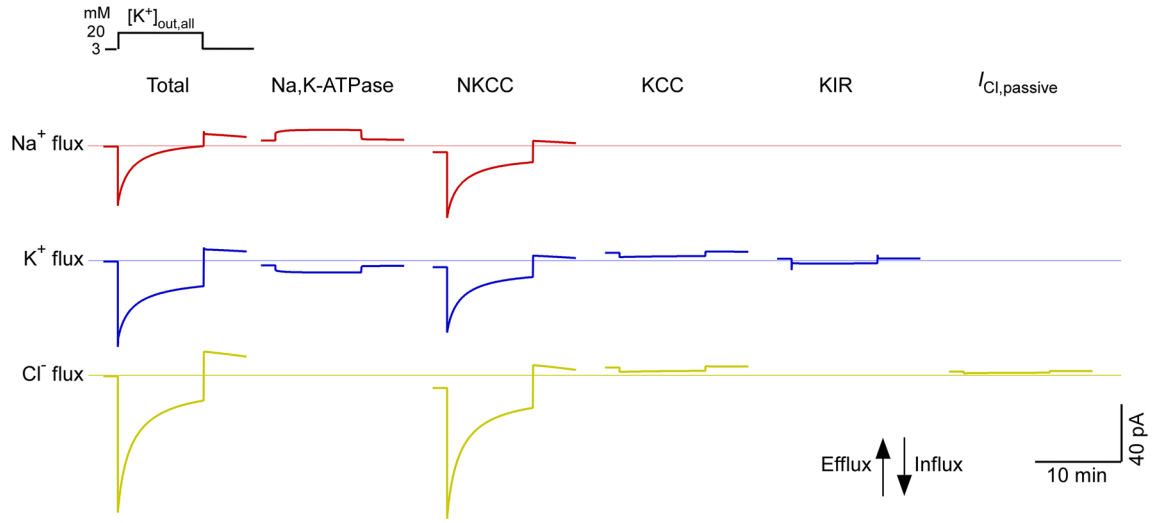

Fig. 4 The contributions of ion channels and transporters to the changes of intracellular ion concentrations in astrocytes. Ion flux of Na^+ (*row 1*, *red lines*), K^+ (*row 2*, *blue lines*), and Cl^- (*row 3*, *yellow lines*) were simulated using the same conditions as in Fig. 3. Results are shown for the total of all channels and transporters (*column 1*), Na,K-ATPases (*column 2*), NKCCs (*column 3*), KCCs (*column 4*), KIR channels, and $I_{Cl,passive}$ (*column 5*). Positive values (*upward*) correspond to an outward flux of ions. *Thin lines* represent zero levels

Table 4 Area under the curve between control and under high $[K^+]_{out}$ conditions

	Total (pA s)	Na,K-ATPase (pA s)	NKCC (pA s)	KCC (pA s)	KIR (pA s)	$I_{Cl,passive}$ (pA s)
Na^+ flux	−4425.8	4274.2	−8700.0	NA	NA	NA
K^+ flux	−15,080.8	−2849.4	−8700.0	−1553.5	−1977.9	NA
Cl^- flux	−19,499.0	NA	−17,399.9	−1553.5	NA	−545.5

Table 5 Ion fluxes through ion channels and transporters under control conditions

	Total (pA)	Na,K-ATPase (pA)	NKCC (pA)	KCC (pA)	KIR (pA)	$I_{Cl,passive}$ (pA)
Na^+ flux	0.0	4.2	−4.2	NA	NA	NA
K^+ flux	0.0	−2.8	−4.2	5.7	1.4	NA
Cl^- flux	0.0	NA	−8.5	5.7	NA	2.8

$[Cl^-]_{in}$ could be primarily accounted for by increased Cl^- influx through NKCCs.

Drug effects on high $[K^+]_{out}$-induced changes in intracellular ion concentrations and swelling

To examine drug effects on astrocytes under high $[K^+]_{out}$ conditions, we examined the effects of blocking Na,K-ATPase, NKCC, and KIR channels on intracellular ion concentrations and swelling using the astrocyte model (Fig. 5). In addition to applying high $[K^+]_{out}$, as in Figs. 3 and 4, we blocked one of the transporters or ion channels and simulated the consequent effects on the $[K^+]_{out}$-induced changes in intracellular ion concentrations and swelling (Fig. 5a). The blocking of Na,K-ATPase had the effect of suppressing swelling to some extent (Fig. 5a, b, column 1). This weaker effect of the Na,K-ATPase blockade compared with that of NKCC is comparable to the experimental finding that ouabain has little effect on the suppression of high $[K^+]_{out}$-induced swelling [54]. Na,K-ATPase pumps Na^+ out and K^+ in. Therefore, the blocking of Na,K-ATPase could increase $[Na^+]_{in}$ and decrease $[K^+]_{in}$ by overcoming the elevation of $[K^+]_{in}$, disrupting intracellular ion balance. The blocking of NKCC suppressed swelling and decreased all of the intracellular ion concentrations (Fig. 5a, b, column 2). These results are comparable to experimental results with the NKCC1 blocker bumetanide [9, 55] and generic ablation of NKCC1 [56]. On the contrary, the blocking of KIR channels (with Ba^{2+}, for example) slightly supressed swelling and increases in $[K^+]_{in}$ and $[Cl^-]_{in}$ regardless the strength of the block (Fig. 5a, b, column 3). Therefore, the blocking of NaKATPase and NKCC effectively suppressed swelling, but their effects on intracellular ion concentrations differed.

K^+ spatial buffering in the non-uniform distribution of high $[K^+]_{out}$

The presence of K^+ spatial buffering by astrocytes has been suggested in a number of studies, although its feasibility, function, and the underlying mechanism are disputed [34, 49]. To study astrocytic K^+ spatial buffering, we applied a non-uniform distribution of high $[K^+]_{out}$ to the astrocyte model, from which we calculated K^+ flux in the synaptic cleft (Fig. 6).

KIR channels in astrocytes are localized at the membrane surrounding the synaptic cleft, and are suggested to be involved in K^+ spatial buffering [15]. First, in order to model hyperexcitation conditions in the brain (e.g., those associated with seizures), we raised $[K^+]_{out}$ to 20 mM only in the synaptic cleft (Fig. 6a). While KIR channels in the synaptic cleft released intracellular K^+ before $[K^+]_{out}$ levels were elevated, and therefore did not contribute to K^+ spatial buffering, following the elevation of $[K^+]_{out}$, the outward flux of K^+ was reversed to the inward flux much stronger than that under the uniform distribution of high $[K^+]_{out}$, and excess K^+ in the synaptic cleft was absorbed into the intracellular spaces of astrocytes (Fig. 6a, KIR [Synaptic cleft]). The K^+ absorption at the synaptic cleft was $[K^+]_{out}$ dependent; as $[K^+]_{out}$ increased, the outward KIR current decreased and finally reversed inwardly (Fig. 6b). This was accounted for by the reversal of membrane potential (V_m) and the equivalent potential of K^+ (E_K). Locally applied $[K^+]_{out}$ in the synaptic cleft depolarized E_K, while membrane potential was clamped by E_K and V_m at the rest parts of the membrane (Fig. 6a, $E_{K,syn}$ and V_m). From this, we estimated that one of the roles of KIR channels localized at the synaptic cleft may be to absorb locally elevated $[K^+]_{out}$.

Next, we examined the drug effects on K^+ uptake (Fig. 7a, b). In this analysis, in addition to high $[K^+]_{out}$ only at the synaptic cleft, 80 % of one of the transporters or ion channels was blocked and K^+ uptake was simulated (Fig. 7a). The blocking of Na,K-ATPase and NKCC slightly decreased KIR currents for K^+ uptake at the synaptic cleft (Fig. 7a, columns 1 and 2, KIR [Synaptic cleft], solid lines). These decreases were enhanced in a block strength-dependent manner (Fig. 7b). However, the blocking of Na,K-ATPase led to continuous decrease in $[K^+]_{in}$ and $[Cl^-]_{in}$, and increase in $[Na^+]_{in}$, whereas the blocking of NKCC resulted in decreases in all of the ion concentrations. The blocking of KIR channels resulted in a substantial loss of K^+ uptake, implying that these channels have a direct effect on K^+ uptake. The complete (100 %) blocking of KIR channels resulted in a complete loss of K^+ uptake.

KIR channels in astrocytes are also known to localize at the membranes surrounding vascular tissues [15, 17, 18, 28, 29]. We next sought to model K^+ flux under conditions in which $[K^+]_{out}$ levels are elevated in a large area of the brain, while the blood–brain barrier remains intact (e.g., under conditions associated with ischemia and anoxia). For this simulation, 20 mM $[K^+]_{out}$ was applied to most of the astrocytic extracellular space, excluding the perivascular regions (Fig. 6c). The elevation of $[K^+]_{out}$ resulted in increases of $[K^+]_{in}$ higher than levels observed with $[K^+]_{out}$ elevation only at the synaptic cleft (Fig. 6, $[K^+]_{in}$). However, accumulated intracellular K^+ was released into perivascular spaces via increases in the outward flow of K^+ through KIR channels (Fig. 6c, KIR [Perivascular]). This increase in K^+ release was not simulated when all $[K^+]_{out}$ levels were elevated. The outward K^+ current was increased as $[K^+]_{out}$ was increased (Fig. 6b). K^+ release through perivascular KIR channels was enhanced by increasing the potential difference between hyperpolarized E_K and depolarized V_m (Fig. 6c, $E_{K,peri}$ and V_m). When all $[K^+]_{out}$ levels were elevated, the potential difference between E_K and V_m did not increase. Therefore, due to differences in the behaviour of E_K and V_m, KIR channels located in the synaptic cleft and perivascular space can redistribute excess K^+.

Finally, we examined drug effects on perivascular K^+ release (Fig. 7c, d). Unlike the drug effects on K^+ uptake, the blocking of Na,K-ATPase and NKCC had opposite effects of slight increases in KIR currents for K^+ uptake at the perivascular space (Fig. 7c, columns 1 and 2, KIR [Perivascular], solid lines). The blocking of Na,K-ATPase and NKCC led to continuous decreases in $[K^+]_{in}$ and $[Cl^-]_{in}$, and opposite changes in $[Na^+]_{in}$ similar to Fig. 7a. The increases in KIR currents were also enhanced in a block strength-dependent manner (Fig. 7d). Conversely, the blocking of KIR channels reduced K^+ release in a block strength-dependent way, as seen in the effects on K^+ uptake (Fig. 7c, d, column 3).

Discussion

In order to reveal the effects of high $[K^+]_{out}$ in the brain, experimental approaches have been used to study high $[K^+]_{out}$-induced increases of intracellular ion concentrations and swelling in astrocytes [8, 9, 32, 45–48]. However, these phenomena result from complex interactions between ion channels and transporters, and, in many cases, previous experimental approaches used have not been suitable for systematically interpreting such complicated interactions. On the other hands, simulation has been used recently to study various physiological phenomena resulting from complex interactions [57, 58]. It was shown that contribution of individual ionic current to complex phenomena can be analyzed by conducting model simulation [59, 60]. Therefore, we constructed

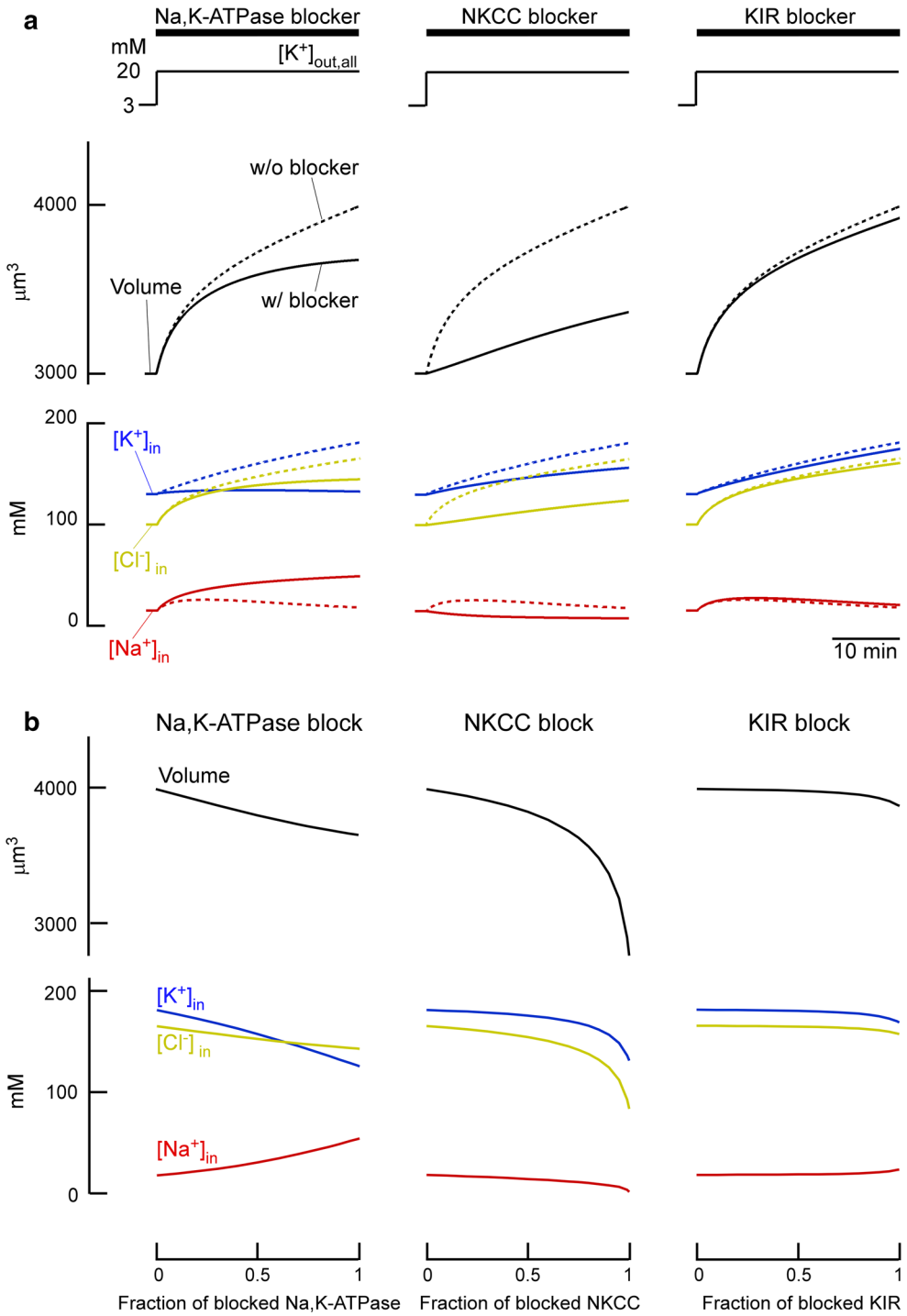

Fig. 5 Simulated drug effects on high $[K^+]_{out}$-induced changes in volume and ion concentration. **a** Simulated drug effects on high $[K^+]_{out}$-induced changes in volume and intracellular ion concentration. The $[K^+]_{out}$ conditions (*row 1*) in Figs. 3 and 4 were used to simulate high $[K^+]_{out}$-induced changes in volume (*row 2*) and intracellular ion concentration (*row 3*) after the blocking of one of the transporters or ion channels. Simulated results are shown separately for 90 % blocks of Na,K-ATPase (*column 1*), NKCC (*column 2*), and KIR channels (*column 3*). Simulation results without blocking are shown as *dotted lines*, and **b** the simulated effects of different block levels on volume and intracellular ion concentration. The effects of various block levels were calculated at the end of 30-min sessions; the results are shown for cell volume (*row 1*) and intracellular ion concentration (*row 2*)

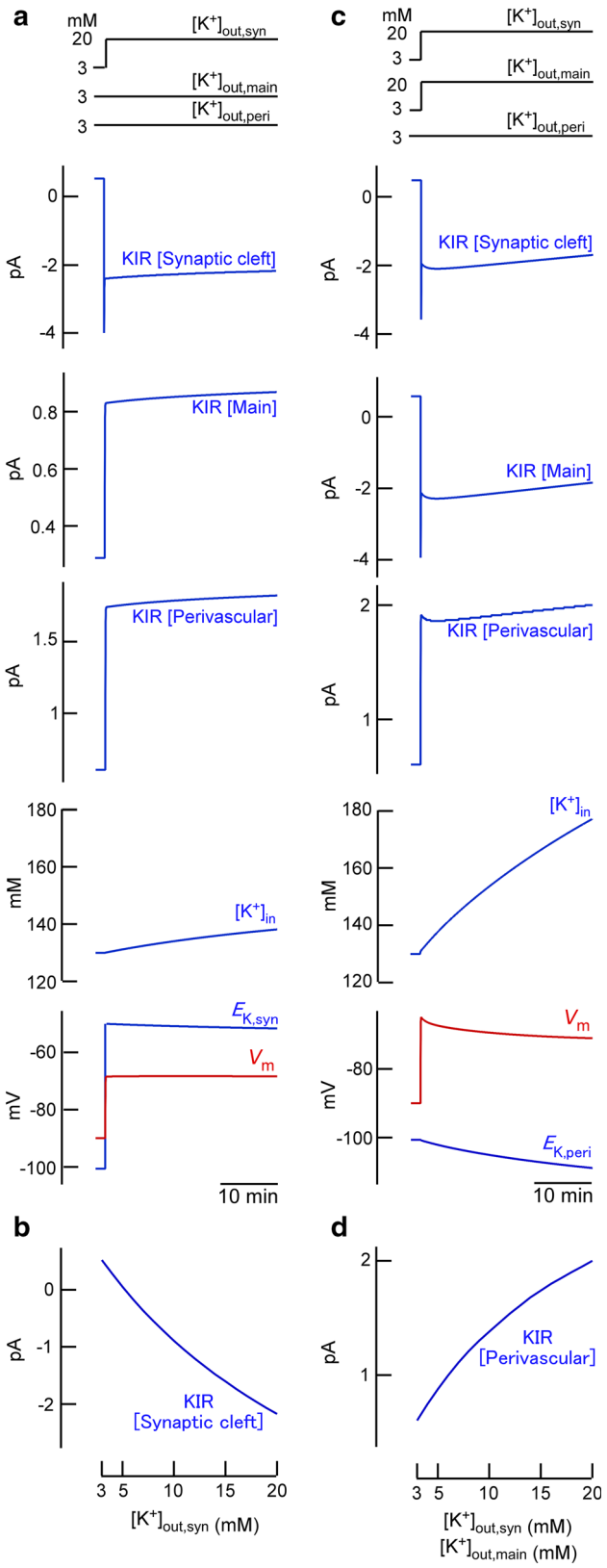

◀**Fig. 6** K^+ spatial buffering in a non-uniform distribution of high $[K^+]_{out}$. **a** Simulated K^+ uptake at the perisynaptic membrane. $[K^+]_{out}$ in the synaptic cleft was increased from 3 to 20 mM ($[K^+]_{out,syn}$). The K^+ currents through the KIR channels at the synaptic cleft, at the main body and at the perivascular endfeet (*KIR [Synaptic cleft]*, *KIR [Main]*, *KIR [Perivascular]*, respectively), intracellular $[K^+]$ ($[K^+]_{in}$), equivalent potential ($E_{K,syn}$), and membrane potential (V_m) at the synaptic cleft are shown. Positive values in K^+ current correspond to the outward direction, **b** $[K^+]_{out}$ dependence of K^+ uptake through KIR channels. K^+ currents through KIR channels at the synaptic cleft (*KIR [Synaptic cleft]*) at various $[K^+]_{out}$ levels were calculated after a 30-min application of high $[K^+]_{out}$, **c** simulated K^+ release into the perivascular space. All $[K^+]_{out}$ levels except $[K^+]_{out,peri}$ were increased from 3 to 20 mM. K^+ currents through KIR channels in the perivascular space are shown (*KIR [Perivascular]*, *KIR [Main]* and *KIR [Perivascular]*). $[K^+]_{in}$, $E_{K,peri}$, and V_m are also shown, as in Fig. 6a, and **d** $[K^+]_{out}$ dependence of K^+ release through KIR channels localized in the perivascular space. K^+ currents through KIR channels in the perivascular space (*KIR [Perivascular]*) at various $[K^+]_{out}$ levels were calculated after a 30-min application of high $[K^+]_{out}$

mathematical models to systemically analyze these complex phenomena in astrocytes.

Analysis with the constructed model showed that K^+ uptake under the uniform distribution of high $[K^+]_{out}$ was primarily affected by the increased activities of Na,K-ATPases and NKCCs (Fig. 4), whereas K^+ spatial buffering under the non-uniform distribution of high $[K^+]_{out}$ was mainly affected by KIR channels localized in the synaptic cleft and perivascular spaces (Fig. 6). In previous experimental studies, it has been disputed whether NKCCs, Na,K-ATPases, or KIR channels contribute to K^+ clearance [49, 50, 55]. One reason for these discrepancies is that these experimental data were interpreted without considering K^+ uptake and K^+ spatial buffering separately. In the present study, we showed that while both NKCCs and Na,K-ATPases can consistently contribute to K^+ uptake under the uniform distribution of high $[K^+]_{out}$, K^+ spatial buffering via the activity of KIR channels requires the non-uniform distribution of high $[K^+]_{out}$. These requirements can explain the discrepancy over the contribution of KIR channels to K^+ clearance and feasibility of the K^+ spatial buffering. For example, several studies have suggested that K^+ clearance occurs predominantly via Na,K-ATPases [6, 7, 61], although the targeted ablation of KIR4.1 channels in astrocytes has also been shown to significantly reduce K^+ clearance [7, 24, 25]. Our results highlight the fact that confusion could arise by interpreting this phenomenon solely in the context of K^+ clearance, without also considering K^+ uptake and K^+ spatial buffering. We found that K^+ uptake was associated with the activity of Na,K-ATPases, NKCCs and KIR channels, but that K^+ uptake

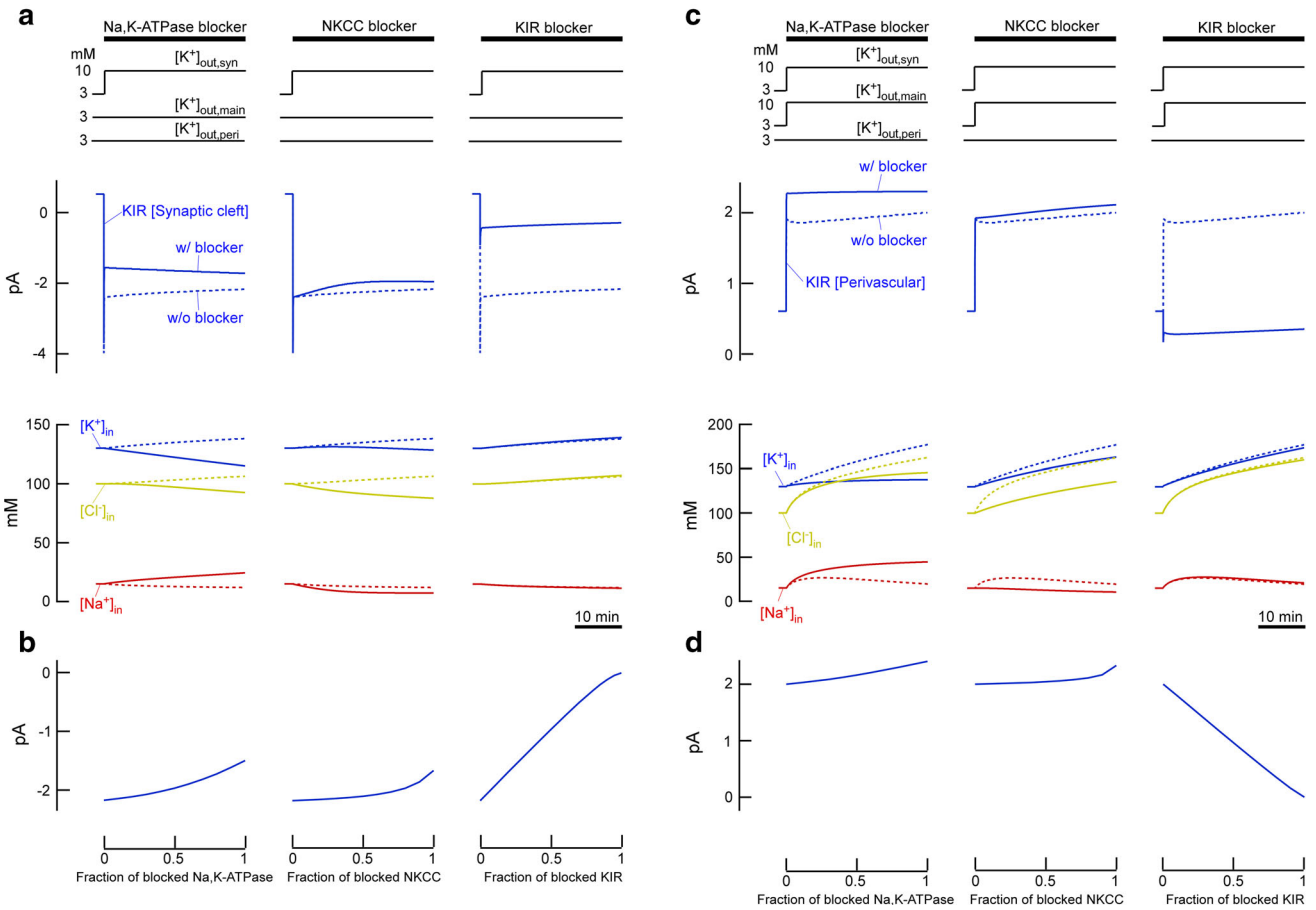

Fig. 7 Simulated drug effects on K^+ spatial buffering in a non-uniform distribution of high $[K^+]_{out}$. **a** Simulated drug effects on KIR currents for K^+ uptake at the perisynaptic membrane. KIR currents and intracellular ion concentrations were simulated under the $[K^+]_{out}$ conditions used in Fig. 6a. Simulation results without blocking are shown as *dotted lines*, **b** simulated effects of various block levels on KIR currents at the perisynaptic membrane. The effects of various block levels were calculated at the end of 30-min sessions, and **c** simulated drug effects on KIR currents for K^+ release into the perivascular space. KIR currents and intracellular ion concentration were simulated under the $[K^+]_{out}$ conditions used in Fig. 6c, and **d** simulated effects of various block levels on KIR currents in the perivascular space. The effects of various block levels were calculated at the end of 30-min sessions

through KIR channels (i.e. inward K^+ current through KIR channels) required the reversal of V_m and E_K due to the elevation of $[K^+]_{out}$ levels. This reversal also explains why KIR4.1 channels with weak inward rectification are selectively expressed in astrocytes, because strong inward rectification would result in the weak inward K^+ current. These observations could explain various contradictions between previous experimental results. For example, it was shown that the targeted ablation of Kir4.1 did not affect the elevation of $[K^+]_{out}$, but instead slowed down the recovery from high $[K^+]_{out}$ [24]. Our data suggest that K^+ uptake is mediated by Na,K-ATPases and NKCCs, which could potentially explain why Kir4.1 ablation was shown to have no effect on the elevation of $[K^+]_{out}$, but instead caused weak K^+ spatial buffering and slow recovery. Therefore, investigations of K^+ clearance should be considered in the context of K^+ uptake and K^+ spatial buffering.

The present analysis also showed that NKCCs have important roles in high $[K^+]_{out}$-induced swelling. Swelling in astrocytes not only underlies cytotoxic edema but also induces cell death by elevating intracellular Ca^{2+} and releasing excitatory amino acids [9, 56, 62]. The effects of blocking NKCCs suggest that NKCCs may be promising targets for the treatment of astrocyte swelling. Indeed, experimental blocking of NKCCs has been shown to suppress high $[K^+]_{out}$-induced swelling and improve recovery from ischemia and anoxia [5, 9, 56, 63–65]. NKCC1 is specifically expressed in astrocytes, and selective NKCC1 blockers are particularly promising. In contrast, the blocking of Na,K-ATPase had the strong side effect of disturbing intracellular ion balance, and the blocking of KIR channels suppressed swelling only slightly. As expected from the direct contributions of KIR channels to K^+ uptake and K^+ release, the blocking of these channels

suppress K^+ uptake and K^+ release. Therefore, the use of channel openers targeting KIR channels may be a more feasible treatment.

In summary, we have shown distinct theoretical responses of ion channels and transporters to high $[K^+]_{out}$ in astrocytes and have elucidated the mechanisms of astrocytic K^+ clearance and swelling. By taking advantage of modeling approaches, we were also able to predict virtual drug effects on astrocytic swelling. These results suggest that future investigations of K^+ clearance by astrocytes should be careful to consider results from such effects in the context of K^+ uptake and K^+ spatial buffering.

Acknowledgments We thank Dr. Hiroshi Hibino, Dr. Fumiaki Nin (Niigata University), and Mr. Hideharu Nagasawa (Osaka University) for critical readings of this manuscript. This work was supported by a grant for 'Research and Development of Next-Generation Integrated Life Simulation Software' from the Ministry of Education, Culture, Sport, Science and Technology of Japan, a Grant-in-Aid for Scientific Research on Innovative Areas (HD Physiology) (22136001) to YK, and a Grant-in-Aid for Scientific Research (C) (25460331) to SM.

Compliance with ethical standards

Conflict of interest None of the authors has any conflict of interest to report.

References

1. Voskuyl RA, ter Keurs HE (1981) Modification of neuronal activity in olfactory cortex slices by extracellular K^+. Brain Res 230:372–377
2. Balestrino M, Aitken PG, Somjen GG (1986) The effects of moderate changes of extracellular K^+ and Ca^{2+} on synaptic and neural function in the CA1 region of the hippocampal slice. Brain Res 377:229–239
3. Kreisman NR, Smith ML (1993) Potassium-induced changes in excitability in the hippocampal CA1 region of immature and adult rats. Brain Res Dev Brain Res 76:67–73
4. Takahashi S, Shibata M, Fukuuchi Y (1999) Role of sodium ion influx in depolarization-induced neuronal cell death by high KCI or veratridine. Eur J Pharmacol 372:297–304
5. Su G, Haworth RA, Dempsey RJ, Sun D (2000) Regulation of Na^+-K^+-Cl^- cotransporter in primary astrocytes by dibutyryl cAMP and high $[K^+]_o$. Am J Physiol Cell Physiol 279:C1710–C1721
6. Xiong ZQ, Stringer JL (2000) Sodium pump activity, not glial spatial buffering, clears potassium after epileptiform activity induced in the dentate gyrus. J Neurophysiol 83:1443–1451
7. D'Ambrosio R, Gordon DS, Winn HR (2002) Differential role of KIR channel and Na^+/K^+-pump in the regulation of extracellular K^+ in rat hippocampus. J Neurophysiol 87:87–102
8. MacVicar BA, Feighan D, Brown A, Ransom B (2002) Intrinsic optical signals in the rat optic nerve: role for K^+ uptake via NKCC1 and swelling of astrocytes. Glia 37:114–123
9. Su G, Kintner DB, Sun D (2002) Contribution of Na^+-K^+-Cl^- cotransporter to high-$[K^+]_o$- induced swelling and EAA release in astrocytes. Am J Physiol Cell Physiol 282:C1136–C1146
10. Newman EA, Frambach DA, Odette LL (1984) Control of extracellular potassium levels by retinal glial cell K^+ siphoning. Science 225:1174–1175
11. Newman EA (1986) High potassium conductance in astrocyte endfeet. Science 233:453–454
12. Takumi T, Ishii T, Horio Y, Morishige K, Takahashi N, Yamada M, Yamashita T, Kiyama H, Sohmiya K, Nakanishi S, Kurachi Y (1995) A novel ATP-dependent inward rectifier potassium channel expressed predominantly in glial cells. J Biol Chem 270:16339–16346
13. Yakushigawa H, Tokunaga Y, Inanobe A, Kani K, Kurachi Y, Maeda T (1998) A novel junction-like membrane complex in the optic nerve astrocyte of the Japanese macaque with a possible relation to a potassium ion channel. Anat Rec 250:465–474
14. Nagelhus EA, Horio Y, Inanobe A, Fujita A, Haug FM, Nielsen S, Kurachi Y, Ottersen OP (1999) Immunogold evidence suggests that coupling of K^+ siphoning and water transport in rat retinal Muller cells is mediated by a coenrichment of Kir4.1 and AQP4 in specific membrane domains. Glia 26:47–54
15. Higashi K, Fujita A, Inanobe A, Tanemoto M, Doi K, Kubo K, Kurachi Y (2001) An inwardly rectifying K^+ channel, Kir4.1, expressed in astrocytes surrounds synapses and blood vessels in brain. Am J Physiol Cell Physiol 281:C922–C931
16. Ishii M, Fujita A, Iwai K, Kusaka S, Higashi K, Inanobe A, Hibino H, Kurachi Y (2003) Differential expression and distribution of Kir5.1 and Kir4.1 inwardly rectifying K^+ channels in retina. Am J Physiol Cell Physiol 285:C260–C267
17. Hibino H, Fujita A, Iwai K, Yamada M, Kurachi Y (2004) Differential assembly of inwardly rectifying K^+ channel subunits, Kir4.1 and Kir5.1, in brain astrocytes. J Biol Chem 279:44065–44073
18. Hibino H, Kurachi Y (2007) Distinct detergent-resistant membrane microdomains (lipid rafts) respectively harvest K^+ and water transport systems in brain astroglia. Eur J Neurosci 26:2539–2555
19. Manley GT, Fujimura M, Ma T, Noshita N, Filiz F, Bollen AW, Chan P, Verkman AS (2000) Aquaporin-4 deletion in mice reduces brain edema after acute water intoxication and ischemic stroke. Nat Med 6:159–163
20. Eid T, Lee TS, Thomas MJ, Amiry-Moghaddam M, Bjornsen LP, Spencer DD, Agre P, Ottersen OP, de Lanerolle NC (2005) Loss of perivascular aquaporin 4 may underlie deficient water and K^+ homeostasis in the human epileptogenic hippocampus. Proc Natl Acad Sci USA 102:1193–1198
21. Binder DK, Yao X, Zador Z, Sick TJ, Verkman AS, Manley GT (2006) Increased seizure duration and slowed potassium kinetics in mice lacking aquaporin-4 water channels. Glia 53:631–636
22. Neusch C, Papadopoulos N, Muller M, Maletzki I, Winter SM, Hirrlinger J, Handschuh M, Bahr M, Richter DW, Kirchhoff F, Hulsmann S (2006) Lack of the Kir4.1 channel subunit abolishes K^+ buffering properties of astrocytes in the ventral respiratory group: impact on extracellular K^+ regulation. J Neurophysiol 95:1843–1852
23. Djukic B, Casper KB, Philpot BD, Chin LS, McCarthy KD (2007) Conditional knock-out of Kir4.1 leads to glial membrane depolarization, inhibition of potassium and glutamate uptake, and enhanced short-term synaptic potentiation. J Neurosci 27:11354–11365
24. Chever O, Djukic B, McCarthy KD, Amzica F (2010) Implication of Kir4.1 channel in excess potassium clearance: an in vivo study on anesthetized glial-conditional Kir4.1 knock-out mice. J Neurosci 30:15769–15777
25. Haj-Yasein NN, Jensen V, Vindedal GF, Gundersen GA, Klungland A, Ottersen OP, Hvalby O, Nagelhus EA (2011) Evidence that compromised K^+ spatial buffering contributes to the epileptogenic effect of mutations in the human Kir4.1 gene (KCNJ10). Glia 59:1635–1642
26. Strohschein S, Huttmann K, Gabriel S, Binder DK, Heinemann U, Steinhauser C (2011) Impact of aquaporin-4 channels on K^+ buffering and gap junction coupling in the hippocampus. Glia 59:973–980

27. Risher WC, Andrew RD, Kirov SA (2009) Real-time passive volume responses of astrocytes to acute osmotic and ischemic stress in cortical slices and in vivo revealed by two-photon microscopy. Glia 57:207–221
28. Simard M, Arcuino G, Takano T, Liu QS, Nedergaard M (2003) Signaling at the gliovascular interface. J Neurosci 23:9254–9262
29. Masaki H, Wakayama Y, Hara H, Jimi T, Unaki A, Iijima S, Oniki H, Nakano K, Kishimoto K, Hirayama Y (2010) Immunocytochemical studies of aquaporin 4, Kir4.1, and alpha1-syntrophin in the astrocyte endfeet of mouse brain capillaries. Acta Histochem Cytochem 43:99–105
30. Jones TA, Greenough WT (1996) Ultrastructural evidence for increased contact between astrocytes and synapses in rats reared in a complex environment. Neurobiol Learn Mem 65:48–56
31. Sasaki H, Sato F, Mannen H (1989) Morphological analysis of single astrocytes of the adult cat central nervous system visualized by HRP microinjection. Brain Res 501:339–354
32. Rose CR, Ransom BR (1996) Intracellular sodium homeostasis in rat hippocampal astrocytes. J Physiol 491(Pt 2):291–305
33. Walz W (2002) Chloride/anion channels in glial cell membranes. Glia 40:1–10
34. Kofuji P, Newman EA (2004) Potassium buffering in the central nervous system. Neuroscience 129:1045–1056
35. Faber GM, Silva J, Livshitz L, Rudy Y (2007) Kinetic properties of the cardiac L-type Ca^{2+} channel and its role in myocyte electrophysiology: a theoretical investigation. Biophys J 92:1522–1543
36. Benjamin BA, Johnson EA (1997) A quantitative description of the Na-K-2Cl cotransporter and its conformity to experimental data. Am J Physiol 273:F473–F482
37. Terashima K, Takeuchi A, Sarai N, Matsuoka S, Shim EB, Leem CH, Noma A (2006) Modelling Cl^- homeostasis and volume regulation of the cardiac cell. Philos Transact A 364:1245–1265
38. Weinstein AM (2010) A mathematical model of rat ascending Henle limb. I. Cotransporter function. Am J Physiol Renal Physiol 298:F512–F524
39. Ostby I, Oyehaug L, Einevoll GT, Nagelhus EA, Plahte E, Zeuthen T, Lloyd CM, Ottersen OP, Omholt SW (2009) Astrocytic mechanisms explaining neural-activity-induced shrinkage of extraneuronal space. PLoS Comput Biol 5:e1000272
40. Lauf PK, Adragna NC (2000) K-Cl cotransport: properties and molecular mechanism. Cell Physiol Biochem Int J Exp Cell Physiol Biochem Pharmacol 10:341–354
41. Meeks JP, Mennerick S (2007) Astrocyte membrane responses and potassium accumulation during neuronal activity. Hippocampus 17:1100–1108
42. Makara JK, Rappert A, Matthias K, Steinhauser C, Spat A, Kettenmann H (2003) Astrocytes from mouse brain slices express ClC-2-mediated Cl^- currents regulated during development and after injury. Mol Cell Neurosci 23:521–530
43. Parkerson KA, Sontheimer H (2004) Biophysical and pharmacological characterization of hypotonically activated chloride currents in cortical astrocytes. Glia 46:419–436
44. Keener J, Sneyd J (1998) Cellular homeostasis. In: Keener J, Sneyd J (eds) Mathematical physiology, 2nd edn. Springer, Berlin, pp 34–73
45. Kimelberg HK, Rutledge E, Goderie S, Charniga C (1995) Astrocytic swelling due to hypotonic or high K^+ medium causes inhibition of glutamate and aspartate uptake and increases their release. J Cereb Blood Flow Metab 15:409–416
46. Ballanyi K, Grafe P, ten Bruggencate G (1987) Ion activities and potassium uptake mechanisms of glial cells in guinea-pig olfactory cortex slices. J Physiol 382:159–174
47. Rose CR, Ransom BR (1997) Gap junctions equalize intracellular Na^+ concentration in astrocytes. Glia 20:299–307
48. Takahashi S, Shibata M, Fukuuchi Y (1997) Effects of increased extracellular potassium on influx of sodium ions in cultured rat astroglia and neurons. Brain Res Dev Brain Res 104:111–117
49. Walz W (2004) Potassium homeostasis in the brain at the organ and cell level. Adv Mol Cell Biol 31:595–609
50. Leis JA, Bekar LK, Walz W (2005) Potassium homeostasis in the ischemic brain. Glia 50:407–416
51. Ianowski JP, O'Donnell MJ (2004) Basolateral ion transport mechanisms during fluid secretion by Drosophila malpighian tubules: Na^+ recycling, Na^+:K^+:2Cl^- cotransport and Cl- conductance. J Exp Biol 207:2599–2609
52. Quraishi IH, Raphael RM (2007) Computational model of vectorial potassium transport by cochlear marginal cells and vestibular dark cells. Am J Physiol Cell Physiol 292:C591–C602
53. Nin F, Hibino H, Murakami S, Suzuki T, Hisa Y, Kurachi Y (2012) Computational model of a circulation current that controls electrochemical properties in the mammalian cochlea. Proc Natl Acad Sci USA 109:9191–9196
54. Vazquez-Juarez E, Hernandez-Benitez R, Lopez-Dominguez A, Pasantes-Morales H (2009) Thrombin potentiates D-aspartate efflux from cultured astrocytes under conditions of K^+ homeostasis disruption. J Neurochem 111:1398–1408
55. Larsen BR, Assentoft M, Cotrina ML, Hua SZ, Nedergaard M, Kaila K, Voipio J, MacAulay N (2014) Contributions of the Na^+/K^+-ATPase, NKCC1, and Kir4.1 to hippocampal K^+ clearance and volume responses. Glia 62:608–622
56. Su G, Kintner DB, Flagella M, Shull GE, Sun D (2002) Astrocytes from Na^+-K^+-Cl^- cotransporter-null mice exhibit absence of swelling and decrease in EAA release. Am J Physiol Cell Physiol 282:C1147–C1160
57. Lim KM, Hong SB, Lee BK, Shim EB, Trayanova N (2015) Computational analysis of the effect of valvular regurgitation on ventricular mechanics using a 3D electromechanics model. J Physiol Sci 65:159–164
58. Kamide T, Okumura S, Ghosh S, Shinoda Y, Mototani Y, Ohnuki Y, Jin H, Cai W, Suita K, Sato I, Umemura M, Fujita T, Yokoyama U, Sato M, Furutani K, Kitano H, Ishikawa Y (2015) Oscillation of cAMP and Ca^{2+} in cardiac myocytes: a systems biology approach. J Physiol Sci 65:195–200
59. Murakami S, Hirose A, Okada YC (2003) Contribution of ionic currents to magnetoencephalography (MEG) and electroencephalography (EEG) signals generated by guinea-pig CA3 slices. J Physiol 553:975–985
60. Okubo C, Sano HI, Naito Y, Tomita M (2013) Contribution of quantitative changes in individual ionic current systems to the embryonic development of ventricular myocytes: a simulation study. J Physiol Sci 63:355–367
61. Ransom CB, Ransom BR, Sontheimer H (2000) Activity-dependent extracellular K^+ accumulation in rat optic nerve: the role of glial and axonal Na^+ pumps. J Physiol 522(Pt 3):427–442
62. Thrane AS, Rappold PM, Fujita T, Torres A, Bekar LK, Takano T, Peng W, Wang F, Rangroo Thrane V, Enger R, Haj-Yasein NN, Skare O, Holen T, Klungland A, Ottersen OP, Nedergaard M, Nagelhus EA (2011) Critical role of aquaporin-4 (AQP4) in astrocytic Ca^{2+} signaling events elicited by cerebral edema. Proc Natl Acad Sci USA 108:846–851
63. Yan Y, Dempsey RJ, Sun D (2001) Na^+-K^+-Cl^- cotransporter in rat focal cerebral ischemia. J Cereb Blood Flow Metab 21:711–721
64. Beck J, Lenart B, Kintner DB, Sun D (2003) Na-K-Cl cotransporter contributes to glutamate-mediated excitotoxicity. J Neurosci 23:5061–5068
65. Kimelberg HK (2005) Astrocytic swelling in cerebral ischemia as a possible cause of injury and target for therapy. Glia 50:389–397